Published in Supercond. Sci. Technol. 26 (2013) 015006, doi:10.1088/0953-2048/26/1/015006

The influence of a grain boundary on the thermal transport properties of bulk, melt-processed Y-Ba-Cu-O

C Marchal[1], J F Fagnard[1], Y H Shi[3], D A Cardwell[3], J Mucha[4], H Misiorek[4], R Cloots[2], B Vertruyen[2] and P Vanderbemden[1]

(1) SUPRATECS and Department of Electrical Engineering and Computer Science B28, Sart-Tilman, B-4000 Liège, Belgium

(2) SUPRATECS and Department of Chemistry B6, Sart-Tilman, B-4000 Liège, Belgium

(3) Bulk Superconductivity Group, Engineering Department, University of Cambridge, Cambridge, CB2 1PZ, UK

(4) W Trzebiatowski Institute for Low Temperature and Structure Research, Polish Academy of Sciences, P.O. Box 1410, 50-950 Wroclaw 2, Poland

E-mail : Philippe.Vanderbemden@ulg.ac.be

Abstract. We report the dependence of thermal conductivity, thermoelectric power and electrical resistivity on temperature for a bulk, large grain melt-processed Y-Ba-Cu-O (YBCO) high temperature superconductor (HTS) containing two grains separated by a well-defined grain boundary. Transport measurements at temperatures between 10 K and 300 K were carried out both within one single grain (intra-granular properties) and across the grain boundary (inter-granular properties). The influence of an applied external magnetic field of up to 8 T on the measured sample properties was also investigated. The presence of the grain boundary is found to affect strongly the electrical resistivity of the melt processed bulk sample, but has almost no effect on its thermoelectric power and thermal conductivity, within experimental error. The results of this study provide direct evidence that the heat flow in multi-granular melt-processed YBCO bulk samples should be virtually unaffected by the presence of grain boundaries in the material.

1. Introduction

Due to their ability to trap large magnetic flux densities [1-3], bulk melt-processed Y-Ba-Cu-O (YBCO) high temperature superconductors (HTS) have a significant potential for a variety of permanent magnet engineering applications such as superconducting rotating machines, flywheel energy storage devices and magnetic bearings [4-8]. The microstructure of melt-processed YBCO bulk monoliths consists generally of

regions of large macroscopic grains, called single domains, separated typically by grain (or domain) boundaries [9]. These natural grain boundaries, which can form during the grain growth of the bulk sample, are often characterized by a high misorientation angle (>10 degrees) [10]. As a result, they are usually characterized by an *inter-granular* critical current density, J_c, which is typically much smaller than the *intra-granular* J_c [11,12]. The presence of grain boundaries has a profound potential impact on the superconducting current flow and magnetic field trapping ability of the material [13-15]. Another parameter affecting the magnetic field trapped by the sample is the generation and propagation of heat that may arise due to the losses caused by large (dB/dt) inherent to the magnetization process [16,17]. Several studies have been undertaken by various groups in order to characterize and predict the temperature increase in bulk superconductors subjected to variable magnetic fields, including AC fields [18-23] or pulsed fields [24-26]. Such investigations, however, require a precise knowledge of the thermal properties of the HTS sample, and, in particular, the thermal conductivity κ as a function of temperature. Although the thermal properties of bulk HTS are relatively well documented in the literature, both for single grain (i.e. containing no grain boundary) [27-31] and polycrystalline materials (i.e. containing a large number of grains and boundaries) [32-34], to our knowledge no attempt has been made to date to characterize the thermal transport properties across *one single grain boundary* in bulk, melt-processed YBCO. Such an investigation is the subject of this paper.

The purpose of the present work is to compare the electrical resistivity and thermal transport properties (specifically thermal conductivity and thermoelectric power) measured within a single domain of bulk melt-processed YBCO material and to compare the results with the same parameters measured across a single, well-definite grain boundary separating two large bulk grains.

2. Experiment

2.1. Sample preparation and microstructure

A bulk, melt-processed large grain YBCO superconductor, consisting of a superconducting $YBa_2Cu_3O_{7-\delta}$ (Y-123) matrix containing discrete Y_2BaCuO_5 (Y-211) inclusions, was fabricated by a conventional top seeded melt growth (TSMG) technique, as described in Refs. [35-36]. The material is characterized by a critical temperature $T_c \sim 91.6$ K, which was determined by an AC magnetic measurement [37]. In order to investigate the role played by grain boundaries, this study focuses specifically on an YBCO bulk melt-processed sample where the nucleation of secondary grains occurred and "natural" grain boundaries formed during the growth process. The microstructure of the melt-processed sample consists usually of grains with ab planes parallel to the top surface of the pellet and grains with the ab plane oriented at a high angle to the sample surface, resulting in the formation of high-angle grain boundaries [38,39]. In the present study, a long, bar-shaped sample ($2.45 \times 2.60 \times 17.05$ mm^3) was cut from the initial melt-processed sample using a wire saw. The resulting specimen contained two large grains separated by a well-defined grain boundary, as shown schematically in Figs 1(a) and 1(b). The grain boundary could be observed clearly using optical microscopy with polarized light (Olympus AH3-UMA) at the top surface of the pellet, as shown in Fig. 1(c).

Different micro- and macro-cracks, parallel to each other, are clearly visible in the grain on the left, whereas the grain on the right is almost featureless. The macro-cracks are likely to develop along the easy-to-cleave ab planes (i.e. parallel to the platelet boundaries) and form during the oxygen annealing process [40]. The fact that such cracks cross the plane of observation for the left-hand grain only suggest that the ab planes of this grain are twisted with respect to the surface, thereby giving rise to a grain boundary with high-angle misorientation.

Further information about the structure the grain boundary and adjacent grains can be derived from the optical polarized light micrograph shown in figure 2(a). The different colour-contrast of the grains results from different crystallographic directions. The Y-211 particles are distributed uniformly in both grains and have an average size of 2-3 μm (with some exceptions, e.g. the "shell-shaped" particle labeled "1" near the top left corner of the figure). The boundary between the grains appears to be straight and thin; its "thickness" cannot be distinguished within the resolution of the micrograph. We could not observe any particular segregation of Y-211 near the grain boundary, or the formation of a Y-211-free zone, as is the case in artificially prepared [001]-tilt boundaries [41]. Interestingly, some Y-211 particles appear to be located *across* the boundary plane (e.g. the oblong particle labeled "2"). In addition, no segregated liquid phase was apparent at the boundary, as is often observed in poorly connected boundaries or in polycrystalline samples [42]. Further investigations were carried out using scanning electron microscopy (Philips XL30 FEG-ESEM). A SEM micrograph of the same zone as Fig. 2(a) is shown in Fig. 2(b). The two Y-211 particles labeled "1" and "2" are a reference for the comparison of both micrographs. Remarkably, the boundary position is very difficult to locate accurately by SEM. The line delimited by two white arrows corresponds to the boundary position as extrapolated from the optical micrograph. The micrograph gives further evidence that joint between the two grains, despite their misorientation, is particularly clean and that no obvious modification of Y-211 size or distribution can be observed in the vicinity of the boundary.

2.2. Electrical and thermal measurements

Both electrical and thermal transport measurements were carried out with a Quantum Design Physical Property Measurement System (PPMS) using the *AC Transport Option* for electrical resistivity and the *Thermal Transport Option* (TTO) for thermal conductivity and thermoelectric power, respectively. A conventional 4-point measurement technique was used for the electrical resistivity measurements, with ohmic contacts made using silver paste. This involved placing voltage contacts both within one grain and across the well-defined grain boundary, as shown schematically Fig. 1(a). Silver epoxy resin was used to attach copper leads to the sample for measurement of thermoelectric power and thermal conductivity. A constant amount of heat was injected into the sample using a heater attached to the top contact (the "heater shoe"), and lateral contacts were used to probe simultaneously the voltage difference (for thermoelectric power) or the temperature difference (for thermal conductivity) using Cernox sensors screwed to the lateral copper leads. As was the case for the resistivity measurements, lateral contacts were placed within the grain

and across the grain boundary. The bottom contact of the sample was screwed to the bottom puck of the TTO (the "cold foot"). A thermal radiation screen was anchored thermally to this sample to provide a thermal sink. All measurements were performed in zero applied magnetic field or under an external DC magnetic field of up to 8 T. The orientation of the superconductor on the sample holder was such that the field was perpendicular to the long axis of the sample for the resistivity measurements and parallel for the thermal measurements. Data were recorded for several temperatures between 300 K and 10 K, using a small, constant sweep rate of –0.1 K/min.

The determination of thermal conductivity and electrical resistivity requires knowledge of the geometric parameters of the sample, with the most significant source of uncertainty arising from the distance between the contacts due to their finite size (attached using either silver paste or epoxy resin). The relative uncertainty is the largest for small inter-contact distances, as is the case for the intra-grain contacts (see Fig. 1): in the present case we estimate the geometrical uncertainty for intra-granular and inter-granular measurements to be 12 % and 8 %, respectively. Since the Seebeck coefficient S is given simply by the ratio of the voltage difference to the temperature difference between the contacts, its measurement is almost not affected by such geometric errors, provided that (i) the same pair of contacts is used for simultaneous voltage and temperature measurement – which was the case in our experiment – and that (ii) the location of the equivalent *thermal* contact is the same as for the *electrical* contact. Although this latter hypothesis would be extremely difficult to prove, we believe it can be reasonably assumed.

A possible significant source of error in the thermal measurements arises from radiation losses between the sample and its environment. These losses are eliminated if the temperature of the magnetic screen is equal to that of the sample. However, this condition is never met since the superconductor exhibits a thermal gradient and the screen of the TTO is anchored thermally to only one side (the cold foot). The consequences for thermal conductivity measurements using the TTO were analyzed recently and discussed in detail by Sebek et al. [43]. The resulting error is shown to be most significant at the highest temperatures (~ 300 K), with the relevant corrections identified by the authors being negligible below temperatures of around 150 K. Note that the thermal transport option of the PPMS allows an optional numerical correction for radiation losses to be made, depending on sample emissivity, geometry, average temperature and temperature gradient. In addition, the magnitude of the correction decreases with decreasing temperature: for the present measurements, the correction would be 7 % of the total thermal conductivity at 300 K and less than 2 % below 200 K. This numerical correction was not applied to the present data since it is approximate and much smaller than the geometrical error of the measurement. The thermal property data obtained by this process was compared with that obtained by another more sensitive experimental arrangement using a stationary heat flux technique [44-46]. This involved surrounding the sample with concentric thermal shields, with the temperature of inner shield monitored by a Constantan-Manganin thermocouple and adjusted to approximately the temperature of the sample holder [44], thereby minimizing the effects of radiation. Measurements in this system, however, could only be performed in zero magnetic field.

Published in Supercond. Sci. Technol. 26 (2013) 015006, doi:10.1088/0953-2048/26/1/015006

3. Results

3.1. Electrical resistivity

Figure 3 compares the electrical resistivity measured both within a YBCO grain ($\rho \parallel ab$-plane: *intra-grain*) and across a natural grain boundary (*inter-grain*). Both superconducting transitions are very sharp ($\Delta T < 1$ K) in zero applied magnetic field (Fig. 3(a)), and exhibit a critical temperature of 91.5 K. These features are characteristic of high quality and well-oxygenated melt-processed YBCO material. The inset of Fig. 3(a), shows that both intra-grain and inter-grain $\rho(T)$ curves display a quasi-linear behaviour in the normal state. However, the normal-state resistivity measured across the boundary is approximately twice that in the grain. The effect of applied DC magnetic fields of up to 8 T ($\parallel c$-axis) is shown in Figs 3(b) and 3(c). The $\rho(T)$ transitions measured within the grain and across the grain boundary are both broadened, shifted to lower temperatures and are clearly distinct. The intra-grain curves (Fig. 3(b)) do not exhibit any points of inflection, whereas the inter-granular data (Fig. 3(c)) display a decrease at T_c followed by a 'foot-like' structure at the bottom of the transition. This feature is a clear signature of the presence of a grain boundary: the initial decrease in $\rho(T)$ arises from the superconducting transition of both grains adjacent to the boundary and the foot is a characteristic of the boundary itself [11].

3.2. Thermal conductivity

Figure 4 compares the temperature dependence of the thermal conductivity $\kappa(T)$ measured both within a YBCO grain ($\kappa \parallel ab$-plane) and across the grain boundary. It is well known that thermal conductivity measurements are susceptible to thermal radiation loss effects [43,46]. As a result, experiments were carried out using two different experimental arrangements: the Physical Property Measurement System with thermal transport option (system 1), allowing $\kappa(T)$ to be measured under DC magnetic fields up to 8 T, and a bespoke measurement system with minimal thermal radiation losses but only for zero applied external magnetic field (system 2).

The thermal property data shown in Fig. 4(a) were measured in zero magnetic field. We first compare the measurements obtained with the TTO device (circles) with those obtained using the home-made system (squares). Fig. 4(a) shows a small quantitative disagreement between the two sets of data, with the intra-and inter-granular data differing by ~ 10 % and ~ 6 %, respectively. It should be emphasized these relative differences are within the error associated with the geometric uncertainty of the voltage contacts (12 % and 8 %, respectively). Apart from these differences, all the curves display very similar qualitative features. The shape and the order of magnitude of thermal conductivity is similar to those reported for high quality YBCO

single crystals [47,48] or melt-processed single grains [28-30]. Fig. 4(a) shows clearly that a break in slope occurs at the critical temperature T_c determined by resistivity data (cf. Fig. 3), as indicated by the arrow. The thermal conductivity data exhibits a well-defined peak at $T \sim 50$ K, and the slope of the curve, $d\kappa(T)/dT$, is negative above T_c. When comparing the intra-granular and inter-granular data, both systems reveal that the thermal conductivity measured across the grain boundary (white) is somewhat smaller than that measured within the grain. The relative difference, however, is of the order of the measurement uncertainty.

Figures 4(b) and 4(c) show how the thermal conductivity κ varies when a magnetic field of 8 T is applied parallel to the direction of the flow of heat. It can be seen that the magnetic field has very little influence on κ. The perceptible (and reproducible) differences observed both in Figs 4(b) and 4(c) are not artefacts of the measurement process since the geometrical error is expected to be the same at 0 and 8 T. In both cases, the thermal conductivity under an applied field is smaller than that in zero applied field.

3.3. Thermoelectric power

The temperature dependence of the thermoelectric power (Seebeck coefficient S), measured both within a grain (|| *ab*-plane) and across a grain boundary, is shown in Fig. 5. We first describe the intra-granular data in the absence of applied magnetic field (black circles, Fig. 5(a)). The thermoelectric power is negative above the superconducting transition temperature and is weakly temperature dependent, and the values of S at 100 K and 300 K (not shown in Fig. 4) are –3.25 μV/K and –3.38 μV/K, respectively. A sharp transition towards the superconducting state ($S \sim 0$) is observed at $T = 91$ K when the temperature is decreased. The superconducting transition is preceded by a negative peak ($S = –4.42$ μV/K) occurring at $T = 92.7$ K. The origin of this peak is discussed below. The measured behaviour across the grain boundary (white symbols) is very similar to that of the grain but with slightly shifted transition and peak temperatures. The superconducting transition temperatures shift to lower temperatures and broaden significantly when a DC magnetic field of up to 8 T is applied to the sample (Figs 5(b) and 5(c)), whereas the amplitude of the peak decreases significantly. The peak is still observable at 5 T for the intra-grain data (Fig. 5(b)), but degenerates into a small “bump” at 8 T. The thermoelectric power does not exhibit any peak at 5 T and above across the grain boundary (Fig. 5(c)).

The inset of Fig. 5(c) shows the inter-granular thermoelectric power across the grain boundary, measured with heat power reduced by 90 %, at the limit of the signal/noise ratio of the experimental system. This results in a lower signal to noise ratio and the disappearance of the negative peak mentioned above. This result provides evidence that, in the present case, the peak appearing in the thermoelectric power above T_c is related directly to the experimental measurement conditions. A discussion about the origin of this peak can be found in the next section.

Published in Supercond. Sci. Technol. 26 (2013) 015006, doi:10.1088/0953-2048/26/1/015006

4. Discussion

In this section we address the influence of the grain boundary in bulk melt-processed YBCO on the electrical and thermal transport properties, with initial focus on electrical resistivity. It is apparent from Fig. 2 that the presence of a single grain boundary has a profound effect on the electrical transport properties of the sample under an applied external magnetic field : the grain resistive transition is sharp without any intermediate step, whereas the grain boundary transition decreases sharply at T_c before leveling off to form a distinct shoulder structure for $T < T_c$. This feature is common to most grain boundaries in high temperature superconductors (see [49] for a review) and underlines the fact that the intergranular J_c is smaller than the intragranular J_c and decreases with the misorientation angle, as shown in previous studies on thin film boundaries deposited on bicrystal substrates [e.g. 50,51] or in artificial boundaries obtained on flux grown bicrystals obtained by multi-seeding [41,52-57]. It should be emphasized that the striking difference in the resistivity within a grain and across the grain boundary confirms, *a posteriori*, that no grain boundaries are present in the former, an that it is indeed a single grain. We note also that the small value of normal-state resistivity at 120 K is 1.5 μΩm for the melt-processed grain. This value is 3-4 times higher than the normal-state resistivity measured in twin-free YBCO single crystals at the same temperature [58] but it is characteristic of high quality melt-processed material [11,59,60]. The normal-state resistivity measured across the boundary is 3.1 μΩm, which is approximately ten times lower than the values obtained for polycrystalline YBCO [33].

We now consider the thermal conductivity κ of the sample (Fig. 4). It has been established by comparing thermal transport data measured using two different experimental arrangements that the value of κ is essentially unaffected by the presence of the grain boundary, within experimental error. It is of interest to estimate the temperature dependence of the electronic thermal conductivity $\kappa_e(T)$ above the critical temperature by assuming the validity of the Wiedemann-Franz law [48], i.e. $\kappa_e(T) = L_0\, T/\, \rho(T)$, where L_0 represents the Lorenz number ($L_0 = 2.44 \times 10^{-8}$ W Ω K^{-2}). The approximately linear behaviour of $\rho(T)$ above T_c corresponds to a temperature-independent electronic thermal conductivity κ_e of 1.91 W/m K and 0.95 W/m K for the grain and across the grain boundary. At 100 K, these electronic contributions correspond to ~ 16 % and 9% of the total thermal conductivity, respectively. It should be noted that the predicted difference of ~ 1 W/m K between the electronic contributions to κ in both cases is in agreement with the small difference measured in the experimental data (cf. Fig. 3). This small difference could therefore be caused by the reduced contribution of the electronic thermal conductivity across the boundary. This interpretation requires further investigation, however, since this is within the experimental error of the experiment. It can be observed further that the amplitude of the peak in the thermal conductivity (16 W/m K) is rather high. Experimentally, the value of this peak is usually related to the normal-state electrical resistivity : materials that exhibit a relatively high normal state resistivity, such as polycrystals, being characterized typically by relatively small values of κ [27, 34] while low resistivity materials exhibit a

significant peak in κ (for example, see ref. [47]). The negative slope of κ(T) above T_c is in agreement with the comprehensive results obtained by Fujishiro et al. on various melt-processed (RE)BCO superconductors for which it was found that the sign of d$\kappa(T)$/dT varies with type of rare-earth ion in (RE)BCO bulk superconductors, and is negative for RE = Y, Gd and positive for RE = Sm, Nd) [30].

We observe that the magnetic field up to 8 T has relatively little effect on the thermal conductivity of melt-processed $YBa_2Cu_3O_{7-\delta}$. Several theories have been developed to explain the influence of magnetic field on the thermal conductivity, including the effect of the *d*-wave parameter in HTS [61]. In the present case, the small influence of the magnetic field on the measured data is likely to be caused by (i) the small contribution from electronic thermal conductivity (as discussed above) and (ii) the orientation of the applied field, i.e. parallel to the thermal gradient in the present experimental arrangement. Here, the vortices do not significantly impede the flow of heat and the scattering of phonons by vortex cores is expected to be small [29]. This feature is in agreement with results obtained on Sm-based melt-processed superconductors under similar experimental conditions [29]. We note also that, unlike the resistivity data, the application of a magnetic field does not produce a distinct dfference in the behaviour of the thermal properties between the grain and grain boundary.

Finally, we discuss the behaviour of the thermoelectric power. Several authors have reported that the room temperature value of the thermoelectric power of YBCO depends empirically on the hole concentration and on the oxygen deficiency δ [62,63]. In the present study, the small and negative room temperature thermoelectric power (for both intra-granular *and* inter-granular measurements) is indicative of a fully oxygenated melt-processed bulk material, since negative values of thermoelectric powers are usually observed in the range $0 < \delta < 0.05$ [62]. We note that this behaviour is observed both within individual grains and across the grain boundary. The similarity between the superconducting transitions in the ρ(T) data measured within the grain and across the grain boundary in zero applied magnetic field (Fig. 3(a)), suggests that oxygen depletion at the grain boundary is small (if any), and this correlates well with the observed strong electrical connectivity between the grains within the resolution of the experiment. We note that the behaviour of the thermoelectric power across the grain boundary is very similar to that measured within the grain, despite a small difference in transition temperatures, which provides direct experimental evidence that the thermoelectric power is not affected significantly by grain boundary scattering effects. Such a result agrees well with those obtained by Carrington et al. on polycrystalline YBCO annealed under different conditions [33].

A remarkable feature of the experimental data shown in Fig. 5 is the appearance of a significant (negative) peak just above the superconducting transition temperature. This peak is suppressed progressively under increasing applied magnetic field. Such an anomalous peak has been observed previously in measurements

of the thermoelectric power and has been explained by superconducting fluctuation effects [64], vortex lattice melting [65] or anisotropy of the thermoelectric power along the *a* and *b* directions in the *ab* plane of the lattice [66]. Extrinsic origins of this peak are either artefacts caused by AC measurement techniques [67, 68] or the existence of small inhomogeneities in T_c in the $YBa_2Cu_3O_{7-\delta}$ superconducting matrix [69, 70]. In the present case, the peak is likely to arise from the magnitude of the thermal gradient used in the measurement, which is larger than the width of superconducting transition (< 0.7 K). This is supported by the fact that the peak almost disappears when, either (i) a magnetic field is applied and the transition is broadened (Fig. 4(b)), or (ii) a much smaller thermal gradient is used (Fig. 5(c)). The disappearance of the peak for both intra-granular and inter-granular transitions also provides clear evidence that this is not an effect related specifically to the grain boundary.

5. Conclusions

We have measured the electrical and thermal transport properties (thermal conductivity and thermoelectric power) in large grain, bulk melt-processed YBCO, both within a single grain and across two grains separated by a well-defined grain boundary. Both resistivity and thermoelectric power measurements indicate a fully oxygenated bulk sample and good connectivity between the two grains. The resistive superconducting transitions are shifted to lower temperatures under applied magnetic fields of a few teslas, and a significant difference in the electrical resistance of the intra-granular and inter-granular measurements appears, whereas the thermal properties within the grain and across the boundary are virtually unaffected by the application of an external magnetic field, at least within experimental error. It can be concluded from the present study that the single grain boundary has a profound impact on the electrical properties of multi-grain YBCO samples, whereas it affects thermal conductivity and thermo-power only very weakly. Such a result gives direct experimental evidence that the presence of one isolated grain boundary in a bulk melt-processed YBCO sample has almost no influence on the flow of heat in the *ab*- plane. As a result, thermal data measured on single grain material can, to good approximation, be used to model and predict the thermal properties of bulk, melt-processed YBCO, even if a few isolated grain boundaries are present in the sample microstructure.

Acknowledgments

We thank the Royal Military Academy (RMA) of Belgium for a cryofluid grant (F07/03). This work is part of an *Action de Recherches Concertées* grant from the Ministry of Higher Education through the Research Council of the University of Liege (ARC 11/16-03). We thank the company Struers for sound advice and technical help. This work is partially funded by a collaboration programme between the FRS-FNRS

(Belgium) and the PAN (Poland). We also thank Prof. M. Ausloos for his constant interest in this work and for many fruitful scientific discussions.

References

[1] Tomita M and Murakami M 2003 *Nature* **421** 517

[2] Eisterer M, Haindl S, Zehetmayer M, Gonzalez-Arrabal R, Weber H W, Litzkendorf D, Zeisberger M, Habisreuther T, Gawalek W, Shlyk L and Krabbes G 2006 *Supercond. Sci. Technol.* **19** S530

[3] Parks D, Weinstein R, Davey K, Sawh R P and Mayes B W 2009 *IEEE Trans. Appl. Supercond*. **19** 1104

[4] Campbell A M and Cardwell D A 1997 *Cryogenics* **37** 567

[5] Jiang Y, Pei R, Xian X, Hong Z and Coombs T A 2008 *Supercond. Sci. Technol.* **21** 065011

[6] Oswald B, Best K J, Setzer M, Soll M, Gawalek W, Gutt A, Kovalev L, Krabbes G, Fisher L and Freyhardt H C 2005 *Supercond. Sci. Technol.* **18** S24

[7] Granados X, Lopez J, Bosch R, Bartolomé E, Lloberas J, Maynou R, Puig T and Obradors X 2008 *Supercond. Sci. Technol.* **21** 034010

[8] Masson P J, Breschi M, Tixador P and Luongo C A 2007 *IEEE Trans. Appl. Supercond*. **17** 1533

[9] Fuchs G, Gruss S, Krabbes G, Schätzle P, Verges P, Müller K-H, Fink J and Schultz L 2000 *Adv in Sol State Phys* **40** 685

[10] Uspenskaya L S, Vlasko-Vlasov V K, Nikitenko V I and Johansen T H 1997 *Phys. Rev. B* **56** 11979

[11] Vanderbemden P, Bradley A D, Doyle R A, Lo W, Astill D M, Cardwell D A and Campbell A M 1998 *Physica C* **302** 257

[12] Küpfer H, Apfelstedt I, Flükiger R, Keller C, Meier-Hirmer R, Runtsch B, Turowski A, Wiech U and Wolf T 1988 *Cryogenics* **28** 650

[13] Jiang X H, Astill D M, Lo W, Cardwell D A, Coombs T A, Campbell A M and Larsen J G 1995 *Physica C* **249** 171

[14] Laurent P, Fagnard J F, Vanderheyden B, Hari Babu N, Cardwell D A, Ausloos M and Vanderbemden P 2008 *Meas. Sci. Technol.* **19** 085705

[15] Iida K, Löwe K, Kühn L, Nenkov K, Fuchs G., Krabbes G, Behr G, Holzapfel B and Schultz L, 2009 *Physica C* **469** 1153

[16] Fujishiro H, Yokoyama K, Kayenama M, Oka M and Noto K 2006 *Physica C* **412** 646

[17] Oka T, Yokoyama K, Fujishiro H and Noto K 2007 *Physica C* **460** 748

[18] Sokolovsky V and Meerovich V 1998 *Physica C* **308** 215

[19] Oka T, Yokoyama K, Fujishiro H and Noto K 2009 *Supercond. Sci. Technol*. **22** 065014

[20] Ogawa J, Iwamoto M, Yamagishi K, Tsukamoto O, Murakami M and Tomita M 2003 *Physica C* **386** 26

[21] Zushi Y, Asaba I, Ogawa J, Yamagishi K and Tsukamoto O 2005 *Cryogenics* **45** 17

[22] Vanderbemden P, Laurent P, Fagnard J F, Ausloos M, Hari Babu N and Cardwell D A 2010 *Supercond. Sci. Technol*. **23** 075006

[23] Laurent P, Fagnard J F, Hari Babu N, Cardwell D A, Vanderheyden B and Vanderbemden P 2010 *Supercond. Sci. Technol.* **23** 124004

[24] Fujishiro H, Kawachi M, Kaneyama M, Fujiwara A, Tateiwa T and Oka T 2006 *Supercond. Sci. Technol.* **19** 540

[25] Berger K, Levêque J, Douine B, Netter D and Rezzoug A 2007 *IEEE Trans. Appl. Supercond.* **17** 3028

[26] Fujishiro H, Naito T, Furuta D 2011 *IEEE Trans. Appl. Supercond.* **21** 2723

[27] Fujiyoshi T, Onuki M, Ohsumi H, Kubota H, Hashimoto M and Miyamoto K 1995 *Synthetic Met.* **71** 1609

[28] Shams G A, Cochrane J W and Russell J G 2000 *Physica C* **336** 205

[29] Fujishiro H and Kohayashi S 2002 *IEEE Trans. Appl. Supercond.* **12** 1124

[30] Fujishiro H, Nariki S and Murakami M 2006 *Supercond. Sci. Technol.* **19** S447

[31] Pekala M, Mucha J, Vanderbemden P, Cloots R and Ausloos M 2005 *Appl. Phys. A* **81** 1001

[32] Bougrine H, Geys J F, Dorbolo S, Cloots R, Mucha J, Nedkov I and Ausloos M 2000 *Eur. Phys. J. B* **13** 437

[33] Carrington A and Cooper J R 1994 *Physica C* **219** 119

[34] Ikebe M, Fujishiro H, Nakasato K, Mikami T, Naito T and Fukase T 1998 *Phys. Stat. Sol. b* **209** 413

[35] Hari Babu N, Kambara M, Shi Y H, Cardwell D A, Tarrant C D and Schneider K R 2002 *Supercond. Sci. Techno.l* **15** 104

[36] Hari Babu N, Iida K, Shi Y and Cardwell D A 2006 *Physica C* **445-448** 286

[37] Vanderbemden P 1998 *Cryogenics* **38** 839

[38] Cloots R, Koutzarova T, Mathieu J-P and Ausloos M 2005 *Supercond. Sci. Technol.* **18** R9

[39] Lo W, Dewhurst C D, Cardwell D A, Vanderbemden P, Doyle R A and Astill D M 1998 *Appl. Supercond.* **4** 507

[40] Diko P and Krabbes G 2003 *Supercond. Sci. Technol.* **16** 90

[41] Bartolomé E, Bozzo B, Granados X, Sandiumenge F, Puig T and Obradors X 2008 *Supercond. Sci. Technol.* **21** 125002

[42] Shi D, Chen J G, Xu M, Cornelius A L, Balachandran U and Goretta K C 1990 *Supercond. Sci. Technol.* **3** 222

[43] Sebek J and Santava E 2009 *J. Phys. Conf. Series* **150** 012044

[44] Jezowski A, Mucha J and Pompe G 1987 *J Phys D* **20** 1500

[45] Mucha J, Dorbolo S, Bougrine H, Durczewski K and Ausloos M 2004 *Cryogenics* **44** 145

[46] Bougrine H, Geys J F, Dorbolo S, Cloots R, Mucha J, Nedkov I and Ausloos M 2000 *Eur. Phys. J. B* **13** 437

[47] Uher C 1990 *J Supercond.* **3** 337

[48] Ikebe M, Fujishiro H, Naito T and Noto K 1994 *J. Phys. Soc. Japan* **63** 3107

[49] Hilgenkamp H and Mannhart J 2002 Rev. Mod. Phys. 74 485

[50] Dimos D, Chaudhari P, Mannhart J and LeGoues F K 1988 *Phys. Rev. Lett.* **61** 219

[51] Feldmann D M, Holesinger T G, Feenstra R and Larbalestier D C 2008 *J. Amer. Ceram. Soc.* **91** 1869

[52] Todt V R, Zhang X F, Miller D J, St. Louis-Weber M and Dravid V P 1996 *Appl. Phys. Lett.* **69** 3746

[53] Prikhna T et al. 2001 *Physica C* **354** 333

[54] Jooss Ch, Bringmann B, Delamare M P, Walter H, Leenders A and Freyhardt H C 2001 *Supercond. Sci. Technol.* **14** 260

[55] Miller D J, Todt V R, St Louis-Weber M, Zhang X F, Steel D G, Field M B and Gray K E 1998 *Mater. Sci. Eng. B* **53** 125

[56] Parikh A, Meyer B and Salama K 1994 *Supercond. Sci.Technol.* **7** 455

[57] Shi Y-H, Durrell J H, Dennis A R, Hari Babu N, Mancini C E and Cardwell D A 2012 *Supercond. Sci. Technol.* **25** 045006

[58] Friedmann T A, Rabin M W, Giapintzakis J, Rice J P and Ginsberg D M 1990 *Phys. Rev. B* **42** 6217

[59] Gao L, Meng R L, Xue Y Y, Hor P H and Chu C W 1991 *Appl. Phys. Lett.* **58** 92

[60] Topal U, Eyyuphan Yakinci M 2010 *Materials Chemistry and Physics* **119** 182

[61] Houssa M and Ausloos M 1997 *J. Phys.: Condens Matter* **9** 201

[62] Cooper J R, Obertelli S D, Carrington A and Loram J W 1991 *Phys Rev B* **44** 12086

[63] Tallon J L, Bernhard C, Shaked H, Hitterman R L and Jorgensen J D 1995 *Phys Rev B* **51** 12911

[64] Howson M A, Salamon M B, Freidmann T A, Inderhees S E, Rice J P, Ginsberg D M and Ghiron K M 1989 *J. Phys.: Condens Matter* **1** 465

[65] Ghamlouch H, Aubin M, Gagnon R and Taillefer L 1996 *Phys. Rev. B* **54** 9070

[66] Lowe A J, Regan S and Howson M A 1991 *Phys. Rev. B* **44** 9757

[67] Ausloos M, Bougrine H, Houssa M and Pekala M 1999 *Phys. Rev. B* **59** 671

[68] Putti M, Cimberle M R, Canesi A, Foglia C and Siri A S 1998 *Phys. Rev. B* **58** 12344

[69] Vidal F, Veira J A, Maza J, Mosqueira J and Carballeira C 1999 in *Materials Science, Fundamental Properties and Future Electronic Applications of High-Tc Superconductors*, Dreschler S L and Mishonov T Editors (Kluwer, Dordrecht)

[70] Mosqueira J, Veira J A and Vidal F 1994 *Physica C* **229** 301

Published in Supercond. Sci. Technol. 26 (2013) 015006, doi:10.1088/0953-2048/26/1/015006

Figure 1

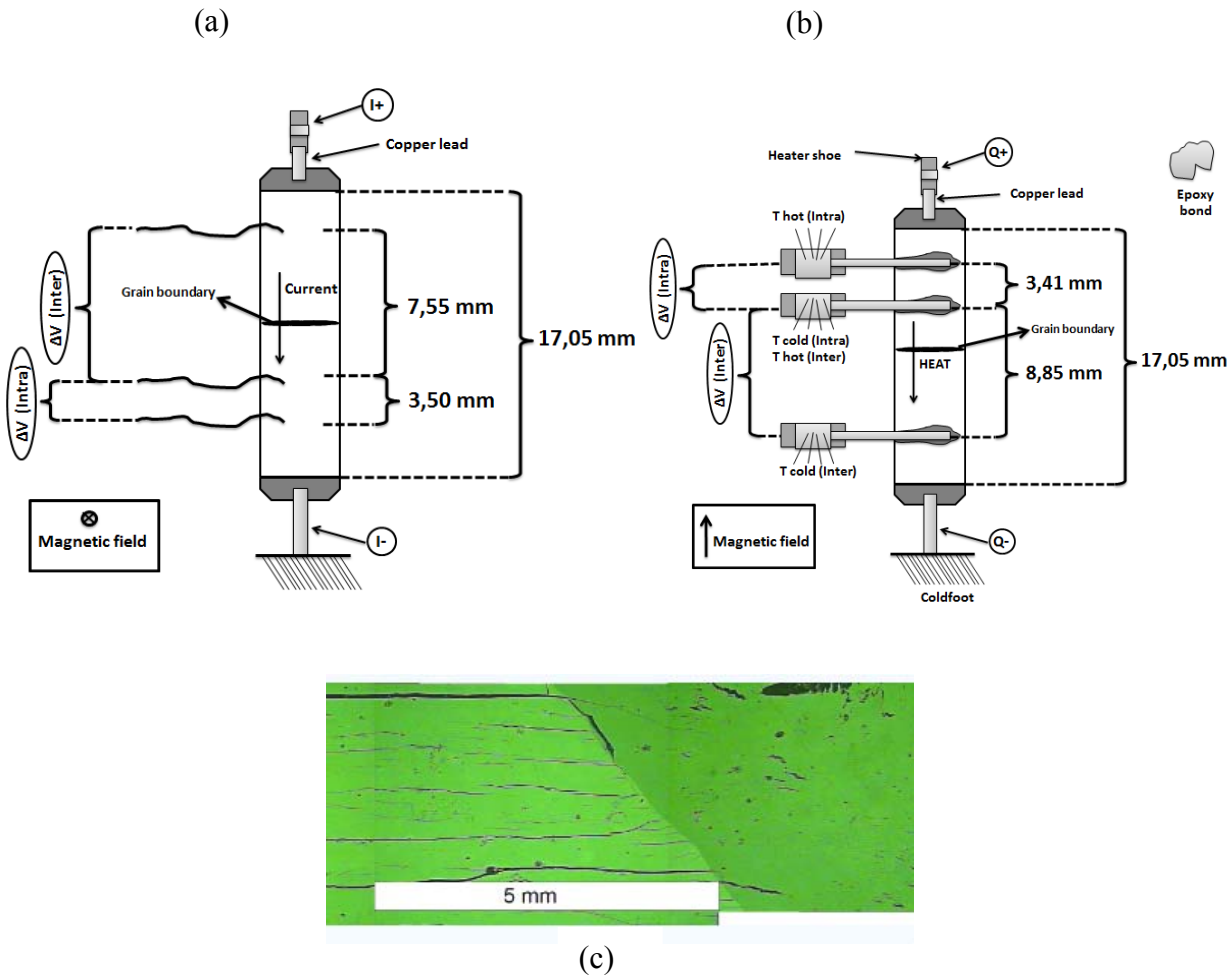

Figure 1. (a) Schematic diagram of the sample prepared for electrical resistivity measurements: the current is injected from I+ to I- and voltage wires are attached by silver paste. The cross section of the sample is 2.45 mm × 2.60 mm. The magnetic field (applied parallel to *c*-axis) is perpendicular to the current. (b) Schematic diagram of the sample prepared for thermal measurements (thermal conductivity and Seebeck coefficient): the heat flux is injected from Q+ (heater shoe) to Q- (cold foot). Temperature sensors are attached to the sample using silver epoxy resin. The magnetic field (parallel to *ab* plane) is applied parallel to the direct of heat flow. (c) Optical polarized light micrograph of the top surface of the melt-textured sample showing the two grains separated by the grain boundary.

Published in Supercond. Sci. Technol. 26 (2013) 015006, doi:10.1088/0953-2048/26/1/015006

Figure 2

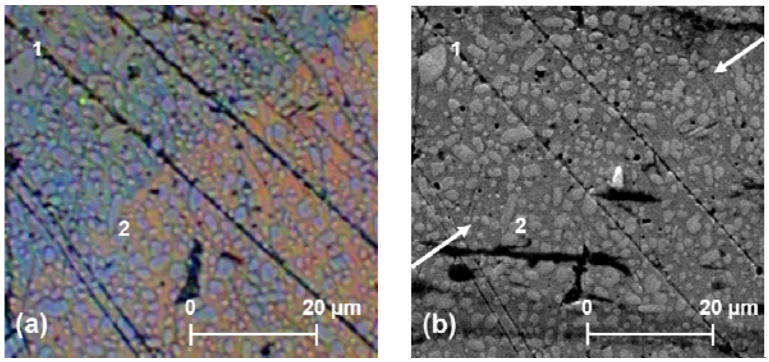

Figure 2. (a) Polarized light optical micrograph of a zone around the grain boundary studied in the melt-textured YBCO sample (b) SEM micrograph of the same zone. The two pairs of parallel lines are micro-scratches that remain after the polishing process. The two arrows show the location of the grain boundary. The numbers 1 and 2 refer to particular Y-211 particles, as discussed in the text.

Published in Supercond. Sci. Technol. 26 (2013) 015006, doi:10.1088/0953-2048/26/1/015006

Figure 3

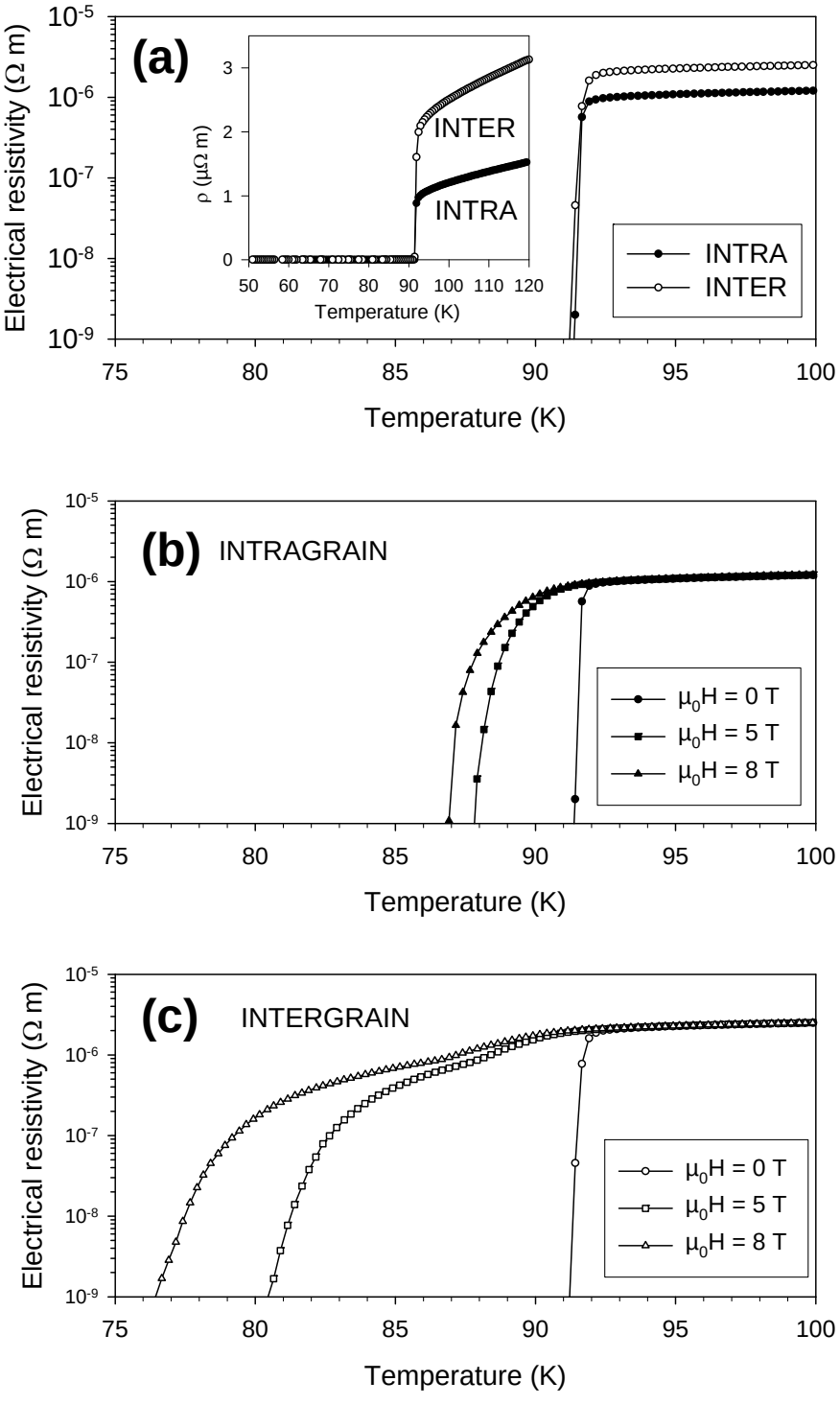

Figure 3. (a) Comparison of the electrical resistivity (logarithmic scale) measured within a YBCO grain and across a grain boundary in zero applied magnetic field. The inset shows the same data plotted using a linear scale for resistivity. (b) Temperature dependence of (b) the intra-granular resistivity and (c) the inter-granular resistivity under DC magnetic fields up to 8 T.

Published in Supercond. Sci. Technol. 26 (2013) 015006, doi:10.1088/0953-2048/26/1/015006

Figure 4

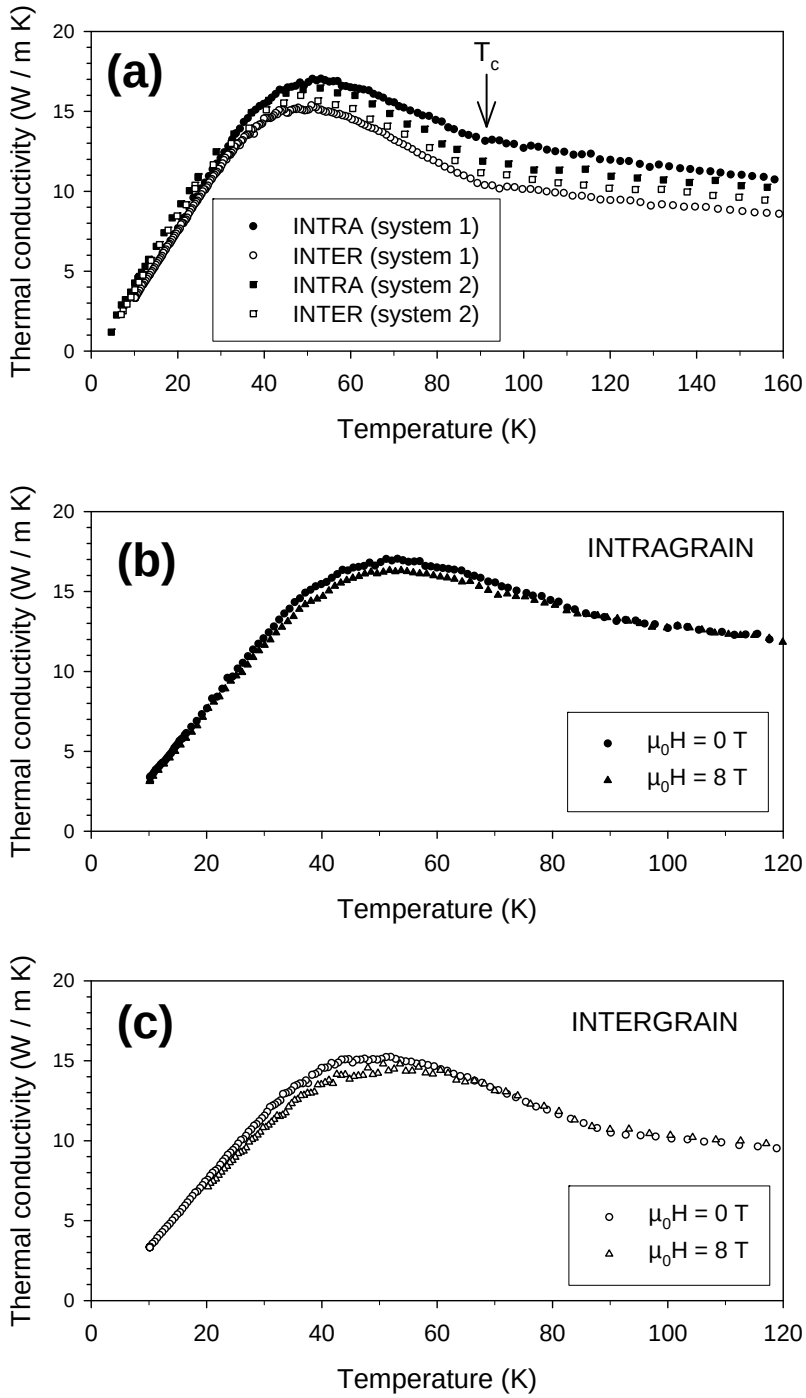

Figure 4. (a) Comparison of the thermal conductivity measured within a YBCO grain and across a grain boundary in zero applied magnetic field, measured using two different experimental arrangements: a Physical Property Measurement System with Thermal Transport Option [TTO] (system 1) and a home-made high-sensitivity system with 3 thermal radiation screens (system 2) (b) Intra-granular thermal conductivity and (c) inter-granular thermal conductivity at 0 and 8 T.

Published in Supercond. Sci. Technol. 26 (2013) 015006, doi:10.1088/0953-2048/26/1/015006

Figure 5

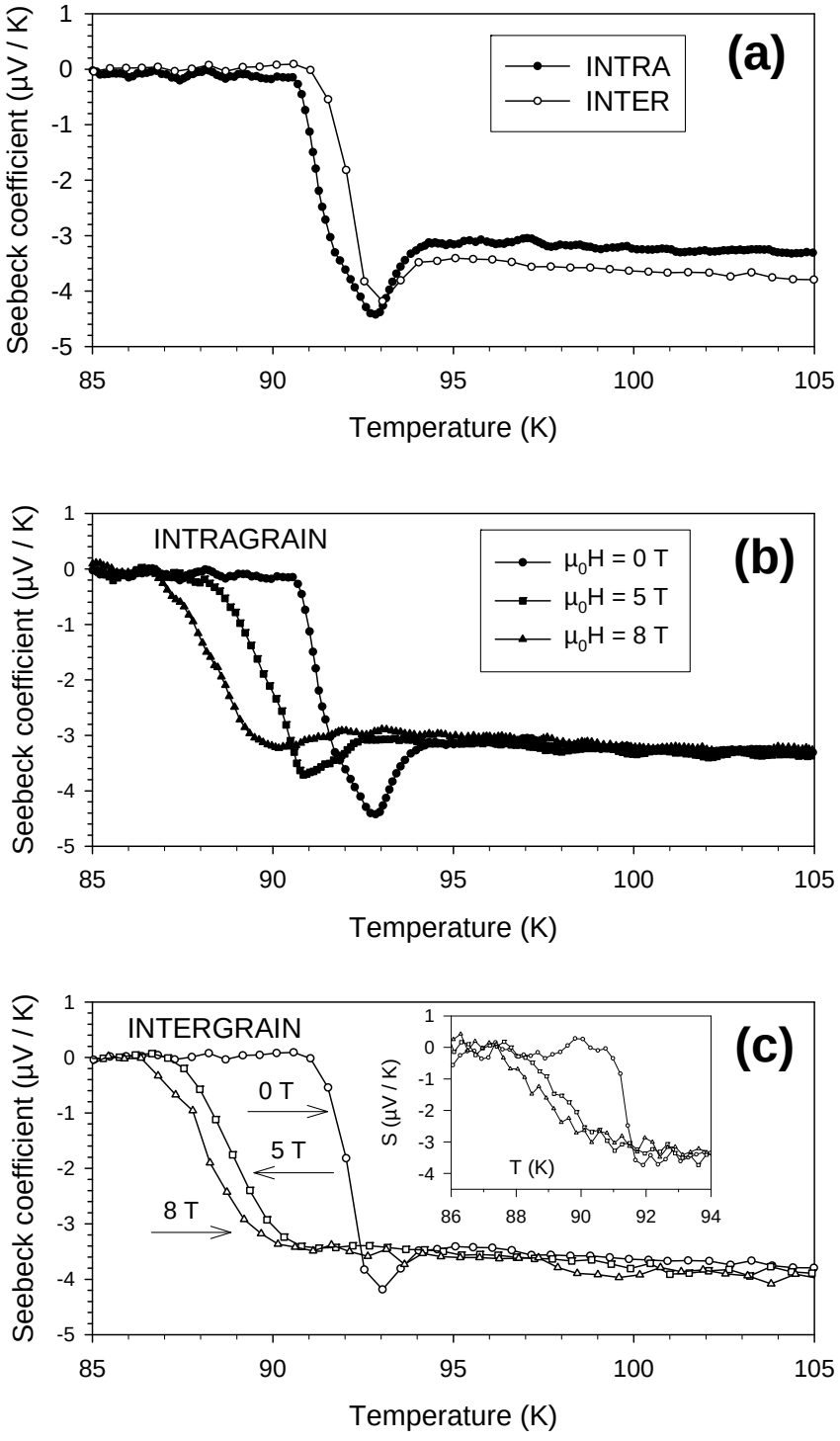

Figure 5. (a) Comparison of the thermoelectric power (Seebeck coefficient) measured within a YBCO grain and across a grain boundary in zero field (b) Intra-granular thermoelectric power and (c) Inter-granular thermoelectric power for several magnetic fields. The inset shows the same data measured with 10% of the heater power.